

Supplementary Information (SI) for Energy & Environmental Science

This Journal is © The Royal Society Chemistry 2025

## **Tailored self-assembled monolayer molecules for perovskite/PERC tandem solar cells with efficiencies over 30%**

So Jeong Park,<sup>‡a</sup> Changhoon Yu,<sup>‡a</sup> Kyu In Shim,<sup>b</sup> Geon Pyo Hong,<sup>a</sup> Sunwu Song,<sup>a</sup> Jae Hyun Park,<sup>ab</sup> Sun Kyung Hwang,<sup>a</sup> Yeo Jin Choi,<sup>a</sup> Jeong Woo Han,<sup>ab</sup> Min Sang Kwon,<sup>\*ab</sup> Ik Jae Park<sup>\*cd</sup> and Jin Young Kim<sup>\*abe</sup>

<sup>a</sup>. Department of Materials Science and Engineering, Seoul National University, Seoul 08826, Republic of Korea

<sup>b</sup>. Research Institute of Advanced Materials (RIAM), Seoul National University, Seoul 08826, Republic of Korea

<sup>c</sup>. Department of Materials Physics, Sookmyung Women's University, Seoul 04310, Republic of Korea

<sup>d</sup>. Institute of Advanced Materials and Systems, Sookmyung Women's University, Seoul 04310, Republic of Korea

<sup>e</sup>. School of Transdisciplinary Innovations, Seoul National University, Seoul 08826, Republic of Korea

\* **Corresponding author:** Min Sang Kwon; **Email:** [minsang@snu.ac.kr](mailto:minsang@snu.ac.kr)

\* **Corresponding author:** Ik Jae Park; **Email:** [parkij@sookmyung.ac.kr](mailto:parkij@sookmyung.ac.kr)

\* **Corresponding author:** Jin Young Kim; **Email:** [jykim.mse@snu.ac.kr](mailto:jykim.mse@snu.ac.kr)

<sup>‡</sup> These authors contribute equally to this work.

## Experimental Section

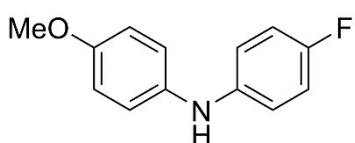
### Materials and methods

#### Materials

Cesium iodide (CsI), lead bromide (PbBr<sub>2</sub>), ammonium thiocyanate (NH<sub>4</sub>SCN), 1,3-propanediammonium iodide (PDAI<sub>2</sub>), lithium fluoride (LiF) Poly(ethyleneimine) (PEIE), *N,N*-dimethylformamide (DMF), dimethyl sulfoxide (DMSO), 2-propanol (IPA), anisole, methyl alcohol, and ethyl alcohol were purchased from Sigma-Aldrich. Formamidinium iodide (FAI) and methylammonium bromide (MABr) were purchased from Greatcell Solar. Lead iodide (PbI<sub>2</sub>), [2-(9H-Carbazol-9-yl)ethyl]phosphonic Acid (2PACz), and [2-(3,6-Dimethoxy-9H-carbazol-9-yl)ethyl]phosphonic Acid (MeO-2PACz) were purchased from TCI.

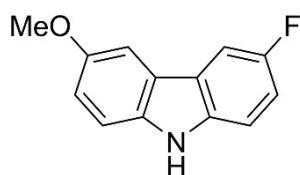
#### Synthesis of SAM molecules

##### 4-Fluoro-N-(4-methoxyphenyl)aniline (*F-1*)



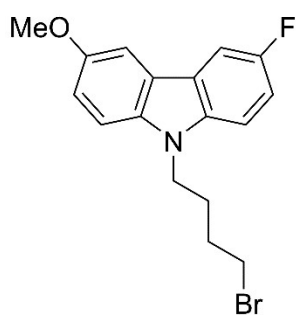
The synthesis procedure for SAM HTL molecules was referenced from the following papers.<sup>1-3</sup> To a two-necked round-bottomed flask, *p*-anisidine (3 g, 24.36 mmol), 4-fluoroaniline (4.69 g, 26.79 mmol), tri-*tert*-butylphosphonium tetrafluoroborate (212 mg, 0.73 mmol), and sodium *tert*-butoxide (4.68 g, 48.72 mmol) were dissolved in anhydrous toluene (45 mL) and purged with N<sub>2</sub> for 15 min. Then, 446 mg of tris(dibenzylideneacetone)dipalladium(0) (0.49 mmol) were added to reaction mixture, then purged again with N<sub>2</sub> for 15 min. After that, the reaction mixture was stirred at 110 °C overnight. Water was added to quench the reaction, then the mixture was extracted with ethyl acetate. The combined organic layer was washed with H<sub>2</sub>O and brine, dried over anhydrous Na<sub>2</sub>SO<sub>4</sub> and concentrated under reduced pressure. The residue was purified by silica gel flash column chromatography using hexanes/EtOAc (9/1 : (v/v)) as the eluent. (Yield 87.5%). <sup>1</sup>H NMR (400 MHz, CDCl<sub>3</sub>) : δ 7.03–6.98 (m, 2H), 6.96–6.83 (m, 6H), 3.79 (s, 3H).

##### 3-Fluoro-6-methoxy-9H-carbazole (*F-2*)



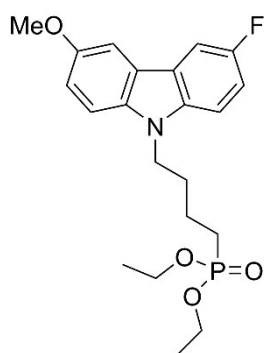
To a mixture of *F-1* (1.63 g, 7.5 mmol), K<sub>2</sub>CO<sub>3</sub> (103 mg, 0.075

mmol) and pivalic acid (6.69 g, 67.5 mmol), Pd(OAc)<sub>2</sub> (50 mg, 0.23 mmol) was added. After that, the uncapped reaction mixture was stirred at 100 °C overnight at ambient pressure of air. The solution is then cooled to rt, diluted with CH<sub>2</sub>Cl<sub>2</sub>. The combined organic layer was washed with H<sub>2</sub>O and brine, dried over anhydrous Na<sub>2</sub>SO<sub>4</sub> and concentrated under reduced pressure. The residue was purified by silica gel flash column chromatography using hexanes/EtOAc (8/1 : (v/v)) as the eluent. (Yield 54.7%). <sup>1</sup>H NMR (400 MHz, CDCl<sub>3</sub>) : δ 7.68 (dd, 1H), 7.47 (d, 1H), 7.36-7.30 (m, 2H), 7.17–7.06 (m, 2H), 3.92 (s, 3H).



9-(4-bromobutyl)-3-fluoro-6-methoxy-9H-carbazole (**F-3**)

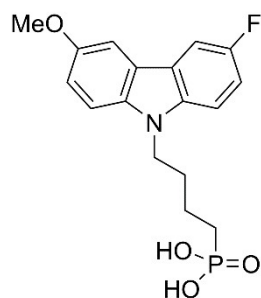
To a solution of *F-2* (400 mg, 1.86 mmol) in 1,4 dibromobutane (9.04 g (5 mL), 41.8 mmol), tetrabutylammonium bromide (283 mg, 0.88 mmol) and 50% KOH aqueous solution (3 mL) were added subsequently. Reaction was stirred at 80 °C for 3 h. After completion of the reaction, extraction was done with dichloromethane. The organic layer was dried over anhydrous Na<sub>2</sub>SO<sub>4</sub> and the solvent was removed under reduced pressure. The crude product was purified by column chromatography using hexanes/EtOAc (10/1 : (v/v)). (Yield 83.0%). <sup>1</sup>H NMR (400 MHz, CDCl<sub>3</sub>) : δ 7.98 (dd, 1H), 7.75 (d, 1H), 7.59 (dd, 1H), 7.54 (d, 1H), 7.27 (td, 1H), 7.11 (dd, 1H), 4.40 (t, 2H), 3.85 (s, 3H), 3.53 (t, 2H), 1.92–1.74 (m, 4H).



Diethyl (4-(3-fluoro-6-methoxy-9H-carbazol-9-yl)butyl)phosphonate (**F-4**)

*F-3* (500 mg, 1.42 mmol) was dissolved in triethyl phosphite (2.44 ml, 14.2 mmol) and the reaction mixture was heated at 150 °C overnight. After reaction completion the solvent was removed under reduced pressure. The crude product was purified by column chromatography using acetone/hexanes (1:3 (v/v)) to give yellowish resin. (Yield 91.4%). <sup>1</sup>H NMR (400 MHz, DMSO-d<sub>6</sub>) : δ 7.97 (dd, 1H), 7.74 (d, 1H), 7.59 (dd, 1H), 7.54 (d, 1H), 7.26 (td, 1H), 7.11 (dd, 1H), 4.37 (t, 2H), 3.95–3.81 (m, 7H), 1.87–1.63 (m, 4H), 1.55–1.37 (m, 2H), 1.14 (t, 6H).

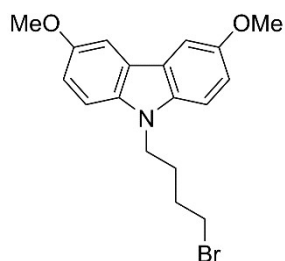
### (4-(3-fluoro-6-methoxy-9H-carbazol-9-yl)butyl)phosphonic acid (**F-MeO-4PACz**)



To a mixture of *F-4* (170 mg, 0.42 mmol) in 1,4-dioxane (7 mL) at room temperature, under N<sub>2</sub> atmosphere, bromotrimethylsilane (0.55 ml, 4.17 mmol) was added dropwise. Then, the mixture was then vigorously stirred at room temperature for overnight. Afterwards, methanol (1 ml) was added and stirring continued for 3 h. Finally, distilled water was added dropwise (10 ml). Then, extraction was done

with ethyl acetate. The combined organic layer was washed with H<sub>2</sub>O and brine, dried over anhydrous Na<sub>2</sub>SO<sub>4</sub> and concentrated under reduced pressure. The product was dissolved in tetrahydrofuran and precipitated into diethyl ether. The product was filtered off and washed with diethyl ether, to give white powder (Yield : 71.8%). <sup>1</sup>H NMR (400 MHz, DMSO-d<sub>6</sub>) : δ 7.97 (dd, 1H), 7.75 (d, 1H), 7.58 (dd, 1H), 7.54 (d, 1H), 7.26 (td, 1H), 7.11 (dd, 1H), 4.36 (t, 2H), 3.85 (s, 3H), 1.87–1.73 (m, 2H), 1.58–1.40 (m, 4H). <sup>13</sup>C NMR (600 MHz, DMSO-d<sub>6</sub>) : δ 156.9, 155.3, 153.0, 136.9, 135.8, 121.9, 115.6, 113.1, 110.4, 110.2, 105.9, 103.5, 55.6, 42.2, 29.6, 27.8, 26.9, 20.4. HRMS (FAB-MS) calculated for [M + H] found: 315.1035.

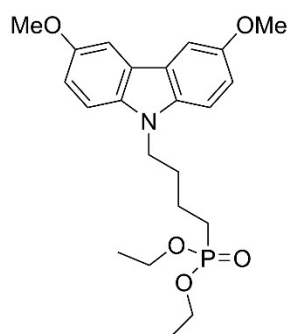
### 9-(4-bromobutyl)-3,6-dimethoxy-9H-carbazole (**O-1**)



To a solution of 3,6-dimethoxy-9H-carbazole (400 mg, 1.76 mmol) in 1,4 dibromobutane (5.0 ml (9.04 g), 41.8 mmol), tetrabutylammonium bromide (283 mg, 0.88 mmol) and 50% KOH aqueous solution (3.0 mL) were added subsequently. Reaction was stirred at 80 °C for 3 h. After completion of the reaction, extraction

was done with dichloromethane. The organic layer was dried over anhydrous Na<sub>2</sub>SO<sub>4</sub> and the solvent was removed under reduced pressure. The crude product was purified by column chromatography using hexanes/EtOAc (5/1 : (v/v)). (Yield 72.1 %). <sup>1</sup>H NMR (400 MHz, DMSO-d<sub>6</sub>) : δ 7.71 (d, 2H), 7.48 (d, 2H), 7.05 (dd, 2H), 4.35 (t, 3H), 3.85 (s, 6H), 3.52 (t, 2H), 1.89-1.73 (m, 4H).

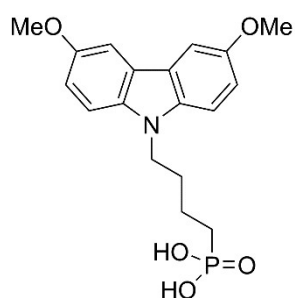
### Diethyl (4-(3,6-dimethoxy-9H-carbazol-9-yl)butyl)phosphonate (**O-2**)



*O-1* (200 mg, 0.55 mmol) was dissolved in triethyl phosphite (1.41 ml, 8.25 mmol) and the reaction mixture was heated at 150 °C

overnight. After reaction completion the solvent was removed under reduced pressure. The crude product was purified by column chromatography using acetone/hexanes (1:2.5 (v/v)) to give yellowish resin. (Yield 82.3 %).  $^1\text{H NMR}$  (400 MHz,  $\text{DMSO-d}_6$ ) :  $\delta$  7.71 (d, 2H), 7.48 (d, 2H), 7.04 (dd, 2H), 4.33 (t, 3H), 3.92-3.86 (m, 4H), 3.85 (s, 6H), 1.84-1.66 (m, 4H), 1.52-1.38 (m, 2H), 1.14 (t, 6H).

#### (4-(3,6-dimethoxy-9H-carbazol-9-yl)butyl)phosphonic acid (**MeO-4PACz**)



To a mixture of *O*-2 (200 mg, 0.48 mmol) in 1,4-dioxane (7 mL) at room temperature, under  $\text{N}_2$  atmosphere, bromotrimethylsilane (0.63 ml, 4.77 mmol) was added dropwise. Then, the mixture was then vigorously stirred at room temperature for overnight. Afterwards, methanol (1 ml) was added and stirring continued for 3 h. Finally, distilled water was added dropwise (10 ml). Then, extraction was done

with ethyl acetate. The combined organic layer was washed with  $\text{H}_2\text{O}$  and brine, dried over anhydrous  $\text{Na}_2\text{SO}_4$  and concentrated under reduced pressure. The product was dissolved in tetrahydrofuran and precipitated into diethyl ether. The product was filtered off and washed with diethyl ether, to give white powder (Yield : 90.0%).  $^1\text{H NMR}$  (400 MHz,  $\text{DMSO-d}_6$ ) :  $\delta$  7.71 (d, 2H), 7.48 (d, 2H), 7.04 (dd, 2H), 4.31 (t, 3H), 3.86 (s, 6H), 1.83-1.73 (m, 2H), 1.57-1.41 (m, 4H).  $^{13}\text{C NMR}$  (600 MHz,  $\text{DMSO-d}_6$ ) :  $\delta$  152.7, 135.5, 122.2, 114.8, 110.0, 103.1, 56.6, 42.1, 29.8, 27.4, 20.4. HRMS (FAB-MS) calculated for  $[\text{M} + \text{H}]$  found: 363.1235.

#### Fabrication of perovskite single-junction solar cells

ITO substrate (AMG Korea Ltd.,  $15 \Omega/\text{sq}$ ) was cleaned with detergent, deionized water, and IPA. Subsequently, the surface was treated by UV-ozone cleaner for 15 min. SAM solution (1 mM in ethyl alcohol) was spin-coated on the ITO substrate at 3000 rpm for 30 s after holding for 10 s, followed by annealing at  $100 \text{ }^\circ\text{C}$  for 10 min. Perovskite precursor solutions were prepared by dissolving FAI, CsI, MABr,  $\text{PbI}_2$ ,  $\text{PbBr}_2$ , and  $\text{NH}_4\text{SCN}$ , molar ratios of which were adjusted to achieve wide-bandgap ( $E_g = \sim 1.68 \text{ eV}$ ,  $\text{Cs}_{0.05}(\text{FA}_{0.77}\text{MA}_{0.23})_{0.95}\text{Pb}(\text{I}_{0.77}\text{Br}_{0.23})_3$  with excess 2 mol%  $\text{NH}_4\text{SCN}$ ), in DMF and DMSO mixed solvent (DMF:DMSO = 4:1 volume ratio). The solution was spin-coated on the SAM film at 3000 rpm for 40 s with an acceleration of 1500 rpm/s. Anisole of 100  $\mu\text{L}$  was dripped in the center of substrates 15 s before the end

of the spin-coating process, and then annealed at 100 °C for 30 min. After that, PDAI<sub>2</sub> solution (1 mM in IPA) spin-coated on perovskite surface at 4000 rpm for 30 s and annealed at 100 °C for 5 min. All solution processes were conducted in the N<sub>2</sub>-filled glove-box. A 15 nm-thick C<sub>60</sub> layer was thermally evaporated at a rate of 0.1 Å s<sup>-1</sup>. PEIE solution (0.2 wt.% in methyl alcohol) was spin-coated at 6000 rpm for 30 s, and a 120 nm-thick Ag electrode was deposited by thermal evaporator at a rate of 1.5 Å s<sup>-1</sup>.

### Fabrication of monolithic perovskite/Si tandem cells

Above the silicon bottom cell, SAM/perovskite/C<sub>60</sub> layers were sequentially assembled. The SAM/perovskite/C<sub>60</sub> layers were formed by the identical method employed for the preparation of single-junction perovskite solar cells. A 50 nm-thick ITO layer was deposited using radiofrequency sputtering system at a rate of 10 nm s<sup>-1</sup>. The sputtering process was conducted through the following condition; room temperature, base pressure of 2.0x10<sup>-6</sup> Torr, working pressure of 2.0x10<sup>-3</sup> mTorr, and power of 50 W. A 500 nm-thick Ag grid was thermally evaporated on the ITO layer using an aligned shadowing mask at a rate of 1.5 Å s<sup>-1</sup>. Lastly, a 105 nm-thick LiF was deposited as an antireflective layer by thermal evaporation at a rate of 1.5 Å s<sup>-1</sup>.

### Density functional theory (DFT) calculations

The calculations of dipole moment, energy level, electron density distribution, and electrostatic distribution of SAMs were conducted to obtain optimized geometry, in vacuum. B3LYP functional and def2-SVP basis set, and dispersion correction with Grimme's Becke-Johnson Damping (D3-BJ) were used in the Gaussian 16. Energy minima were confirmed via vibrational calculations, by the absence of imaginary frequencies.

The calculations about SAMs-perovskite adsorptions were performed using the Vienna *ab Initio* Simulation Package (VASP)<sup>4</sup> and the Jaguar software (Schrodinger, New York, NY) equipped with an optimization tool.<sup>5, 6</sup> For optimization of SAM-Molecules, the Jaguar software was used. In details, the B3LYP hybrid DFT method and the basis set of 6-31G(d) were used. Conformational analysis was performed using the Conformational Search tool from

the MacroModel package with the OPLS-2005 force field to explore the possible initial configurations for the quantum chemical calculations. Energy convergence was set to energy change  $<5 \times 10^{-5}$  hartree and root-mean-square density matrix change  $<5 \times 10^{-6}$  hartree. Moreover, the structures were optimized freely using redundant internal coordinates with the default Schlegel guess. Resulting optimized configurations were used as input configurations for further DFT calculations using VASP. For VASP calculations, the Perdew-Burke-Ernzerhof (PBE) functional of the generalized gradient approximation (GGA) was used for the exchange-correlation energies.<sup>7,8</sup> The energy cut-off for the plane-wave basis set was set to be 520 eV, and a supercell of graphene containing  $3 \times 3$  unit cells with four slab layers with Pb-I termination was selected to model FAPbI<sub>3</sub> systems. Monkhorst-Pack  $2 \times 2 \times 1$  *k*-point meshes were sampled for bulk and surface models. For the structural optimization, all atoms were relaxed except for bottom two slab layers using a conjugate-gradient algorithm until the difference in the total force was  $< 0.03$  eV/Å with the convergence criterion of total energy of  $10^{-4}$  eV, and spin polarization was taken into considerations.<sup>9</sup> Additionally, about 15 Å vacuum layer spacing was adopted, and the DFT-D3 empirical correction method was employed to describe van der Waals interactions.<sup>10</sup> Lastly, VESTA package was used for structural visualization.<sup>11</sup>

### Material characterizations

The synthesized thiol-based hardeners were determined using a <sup>1</sup>H NMR spectrometer (JNM-ECX400 (400 MHz), JEOL), and <sup>13</sup>C NMR spectrometer (AVANCE 600 (600 MHz), Bruker) with CDCl<sub>3</sub> or DMSO-d<sub>6</sub>. TGA measurement was conducted on a PerkinElmer TGA 4000 with N<sub>2</sub> as the purge gas. The scanning rate was 10 °C min<sup>-1</sup> and the scanning range was from 0 to 600 °C. For each measurement, about 5–10 mg of samples was weighed for the analysis. UV/Vis absorbance measurements were done with a UV-Vis-NIR spectrometer (V-770, JASCO). The spectrum of SAM molecules was measured in DMF solvent (20 μM). To characterize the microstructure and morphology of thin film, images of top-view or cross-section were obtained using a field-emission scanning electron microscopy (FE-SEM, MERLIN Compact, ZEISS). The crystallographic analysis of perovskite films was conducted by an X-ray diffractometer (XRD, D8 Advance, Bruker). The absorbance and bandgap derived from Tauc plot were measured through a UV-Vis-NIR spectrometer (Cary-6000i, Agilent). To

identify the work function and valence band energy level, an ultraviolet photoelectron spectroscopy (UPS, VersaProbeIII, ULVAC-PHI) was employed. A steady-state (SS) and time-resolved (TR) photoluminescence (PL, FlouTime 300, PicoQuant) measurement were conducted to analyze defect-assisted non-radiative recombination and charge extraction regarding the variable SAMs. The potential distribution of SAMs was investigated by using Kelvin probe force microscopy (KPFM, NX-10, Park systems) analysis.

### Buried surface characterizations

For perovskite bottom surface analysis, the glass substrate coated with epoxy was combined to the perovskite surface, and then left overnight. By physically detaching, bottom surface of perovskite was obtained. A grazing incidence X-ray diffractometer (GIXRD, D8 Advance, Bruker) patterns were acquired in order to analyze residual stress on bottom surface of perovskite. An X-ray photoelectron spectrometer (XPS, VersaProbeIII, ULVAC-PHI) was performed to investigate the binding energy shift at the buried interface.

### Device characterizations

To obtain the cross-sectional image of the perovskite/Si tandem cell, a specimen was prepared using FIB (Nova Nanolab, FEI), and the image analysis was conducted using TEM (JEM-2100F, JEOL). The current density-voltage ( $J-V$ ) curves of single-junction cells and tandem cells were acquired using solar simulator (PEC-L11, Peccell Technologies, AAA graded) under AM 1.5G illumination ( $100 \text{ mW cm}^{-2}$ ) and ambient condition ( $25 \text{ }^\circ\text{C}$ ,  $\text{RH} < 40\%$ ). The AM 1.5G illumination was calibrated by standard Si cell (91150V, Newport). The aperture size of devices was defined by metal mask;  $0.14 \text{ cm}^2$  for single-junction cells and  $1 \text{ cm}^2$  for tandem cells, respectively. The scan rates of  $J-V$  measurement were  $120$  and  $240 \text{ mV s}^{-1}$  for single junction cells and tandem cells, which was performed under ambient condition at room temperature. The stabilized power output (SPO) of devices was also measured using same equipment. The external quantum efficiency (EQE) spectrum of devices was obtained using a quantum-efficiency measurement system (QUANTX-300, Oriel). The EQE spectra of single-junction solar cells were measured without light and electrical bias. For EQE spectra of tandem cells, perovskite top cell was measured under inducing infrared light bias with an electrical

bias, and then Si bottom cell was measured under inducing blue light bias with an electrical bias. The long-term stability of the semi-transparent perovskite cell was conducted by continuous illumination with a white LED (MWHLP1, THORLABS). The LED light intensity was adjusted to produce the same current density at zero bias as acquired in the  $J-V$  curve (1-sun equivalent). During continuous illumination, the output current density of the cells was monitored under a constant electrical bias close to the maximum power point (MPP). The cell was tested in a chamber filled with nitrogen gas, maintaining a constant temperature of 25 °C and 65 °C using a cooler (ISOS-L-1I and ISOS-L-2I protocols, respectively).

## Supplementary Figures

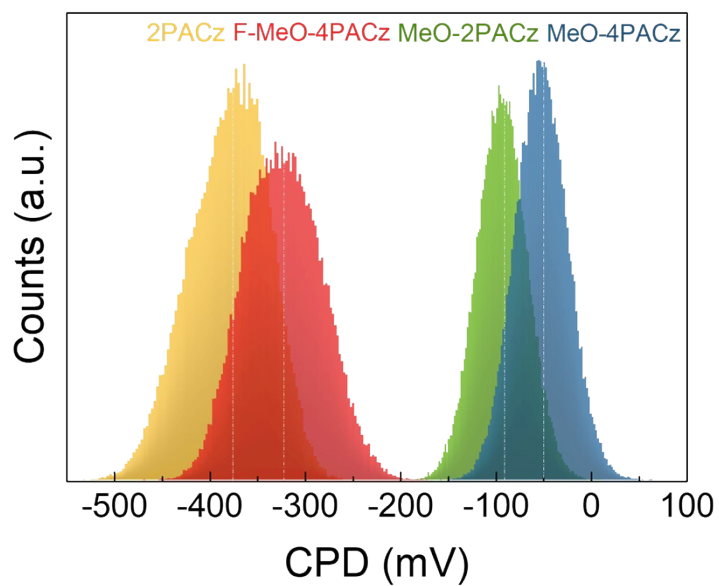


**Fig. S1** Contact potential difference of the ITO/various SAMs film obtained from KPFM analysis.

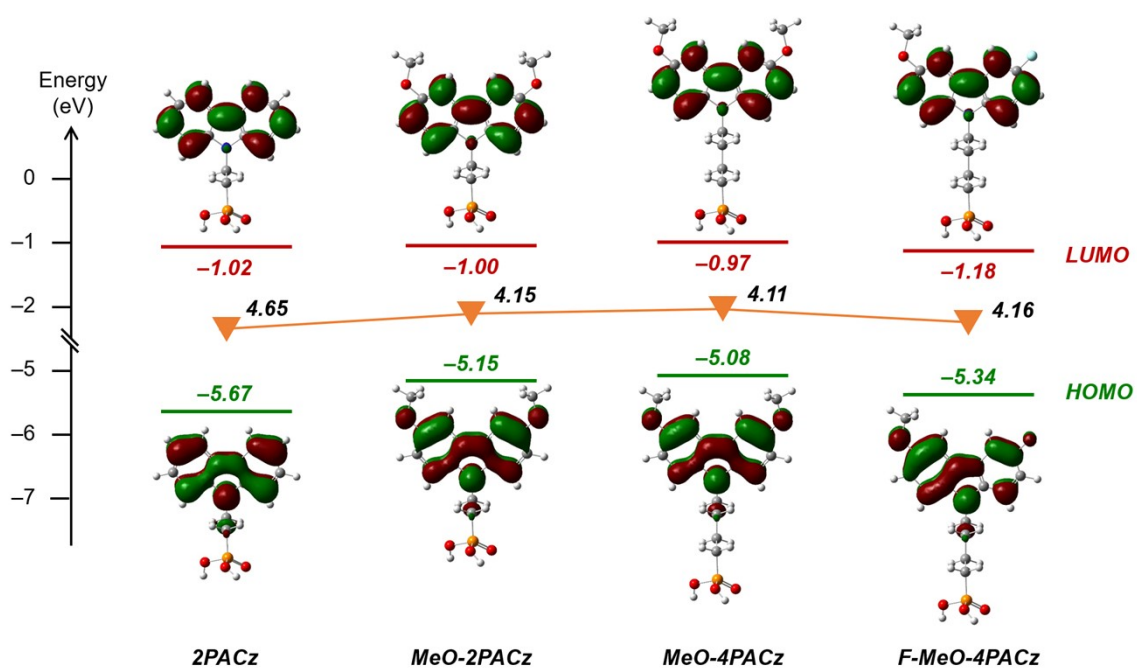


**Fig. S2** Calculated energy band level and electron density distribution of the various SAMs.

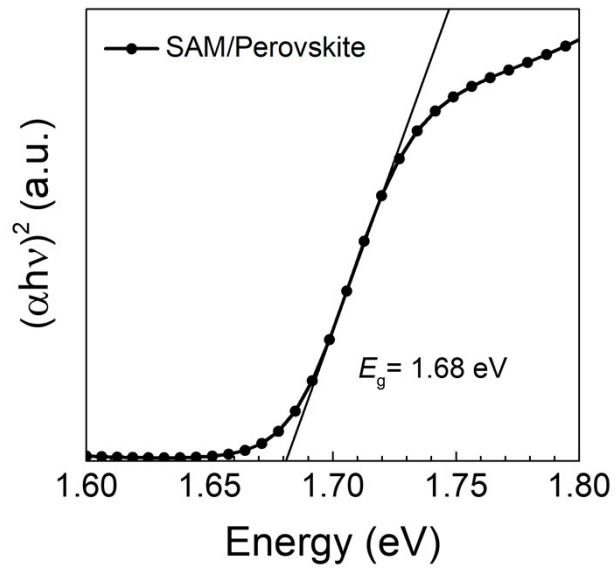


**Fig. S3** Tauc plot of the perovskite thin film (ITO/SAM/perovskite).

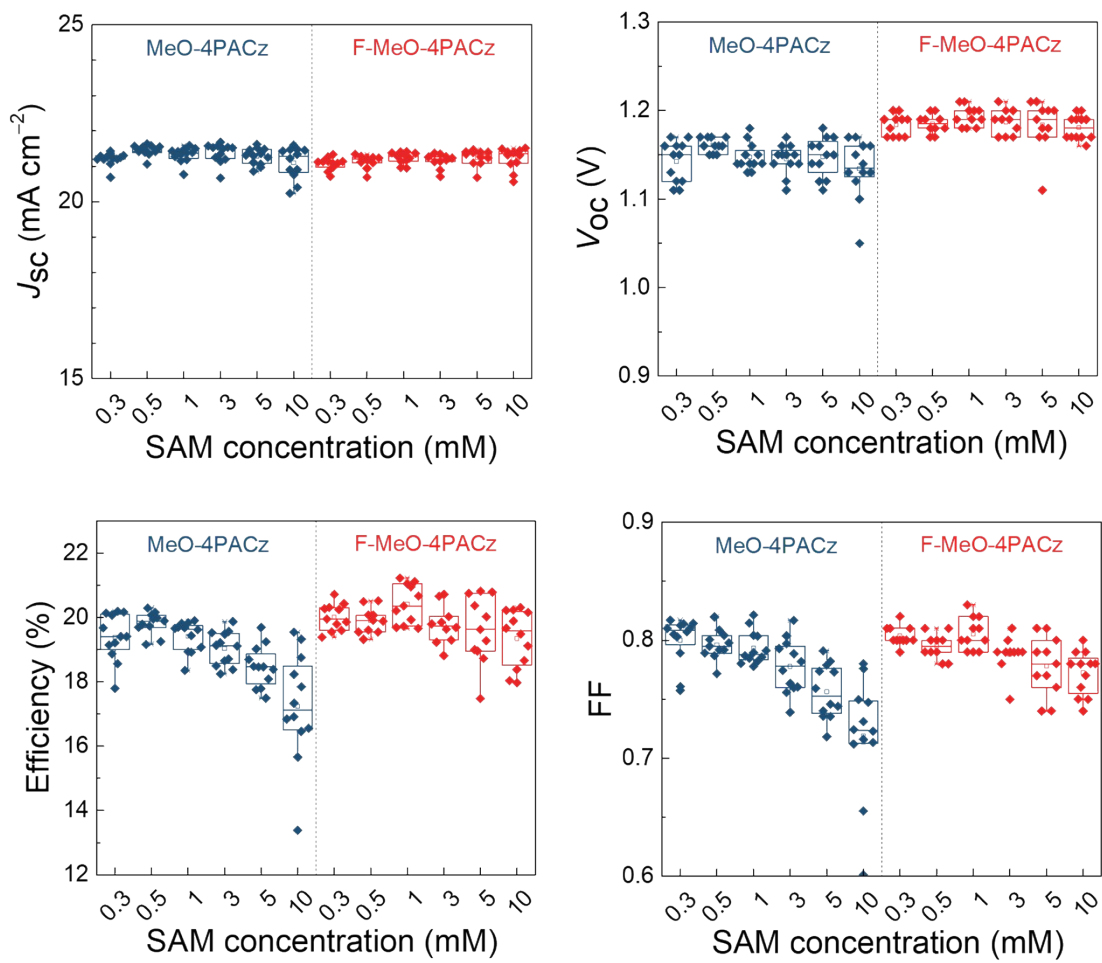


**Fig. S4** Optimization of SAMs concentration in the perovskite single-junction solar cells.

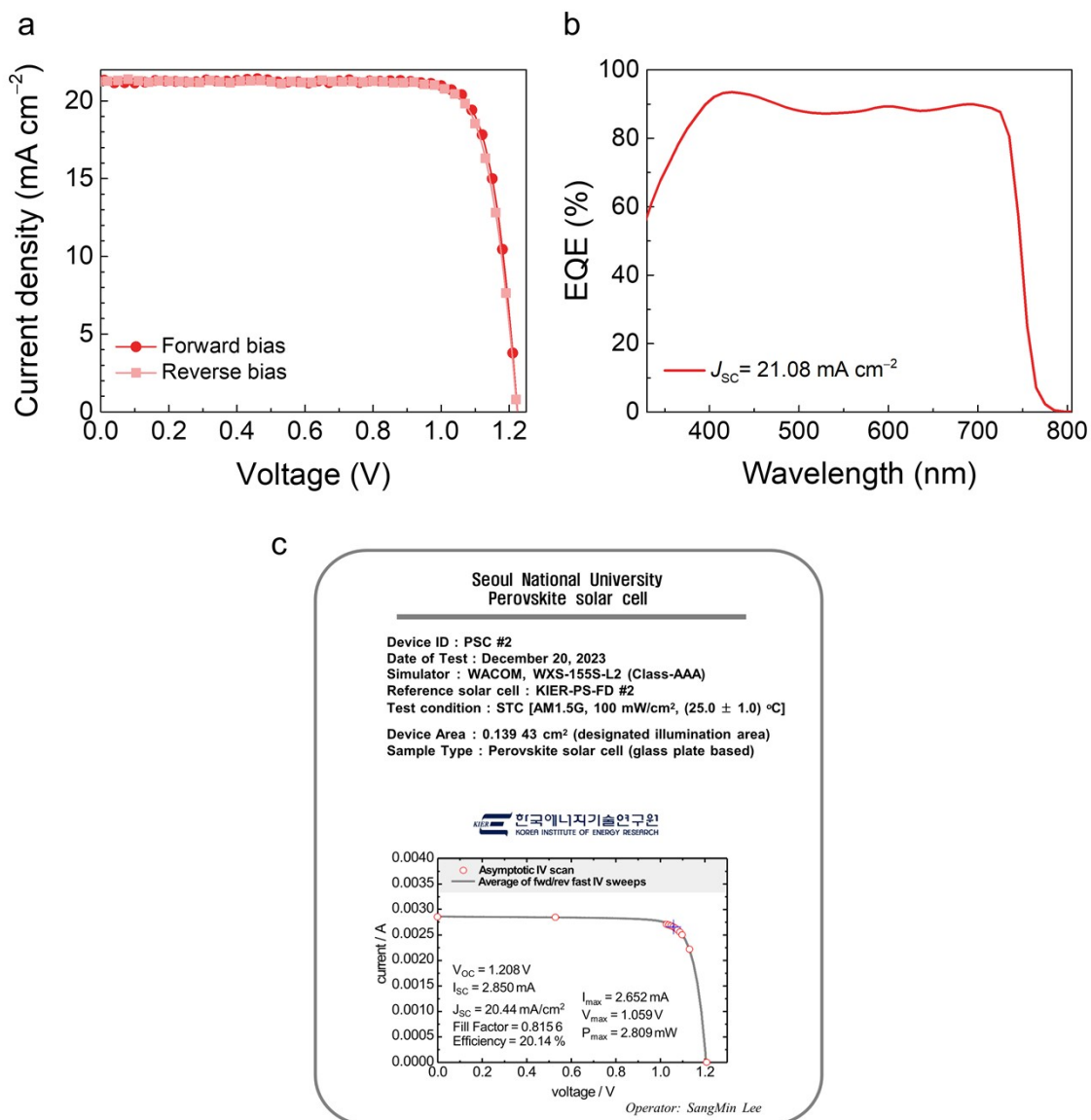


**Fig. S5** (a)  $J$ - $V$  hysteresis, (b) EQE spectrum, and (c) certificated efficiency measured by Korea Institute of Energy Research (KIER) of the F-MeO-4PACz-based single-junction perovskite solar cell.

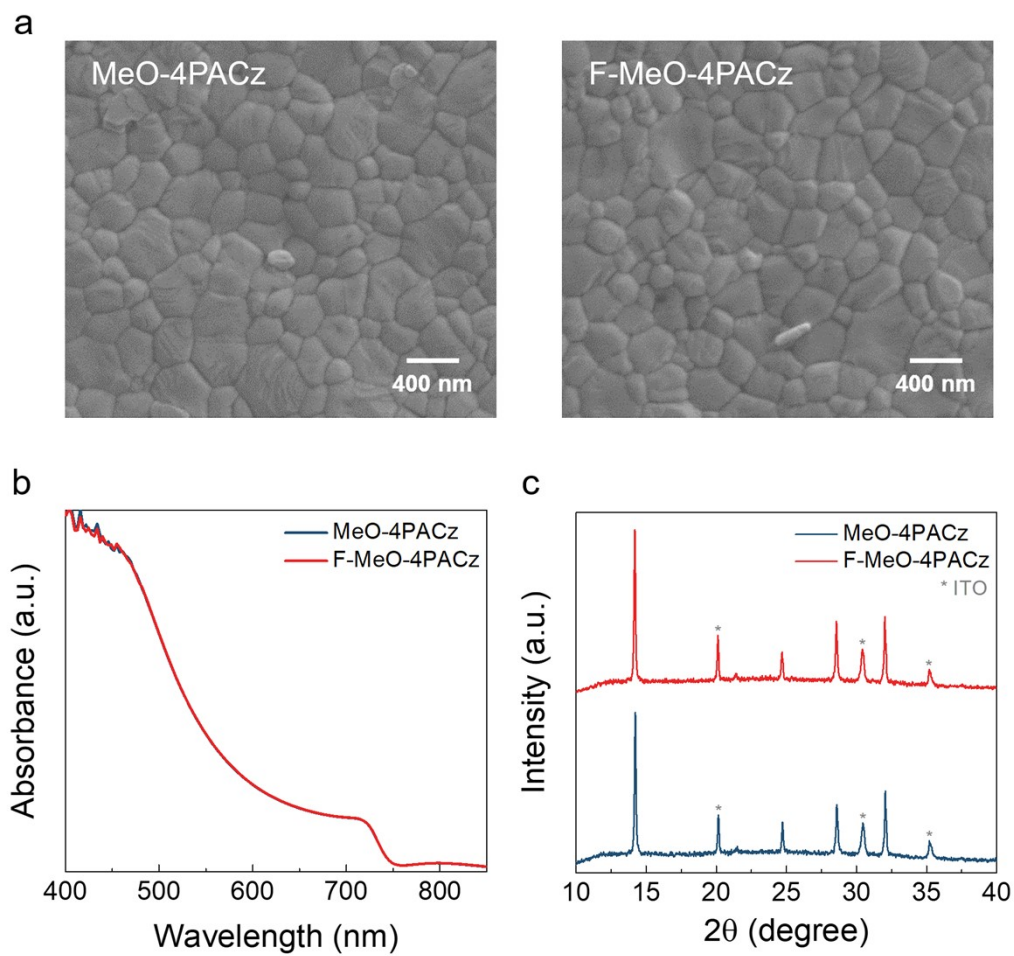


**Fig. S6** (a) Plane-view SEM images, (b) UV-Vis absorption spectra, and (c) XRD spectra of the perovskite films deposited on MeO- and F-MeO-4PACz.

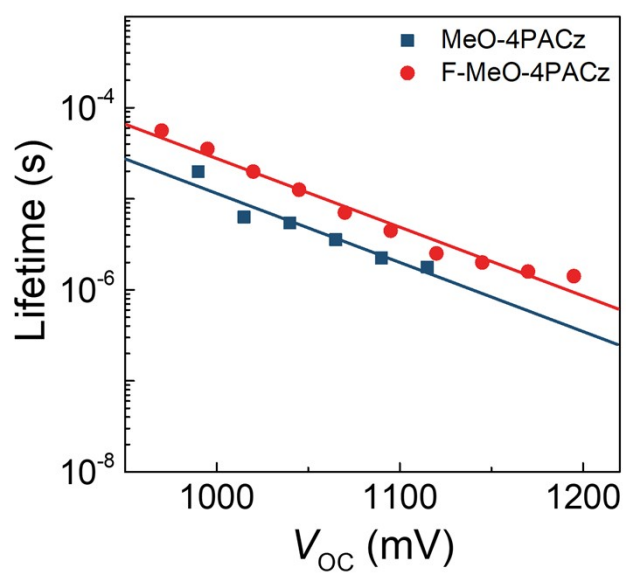


**Fig. S7** TPVD plots of the perovskite single-junction solar cells with different SAMs.

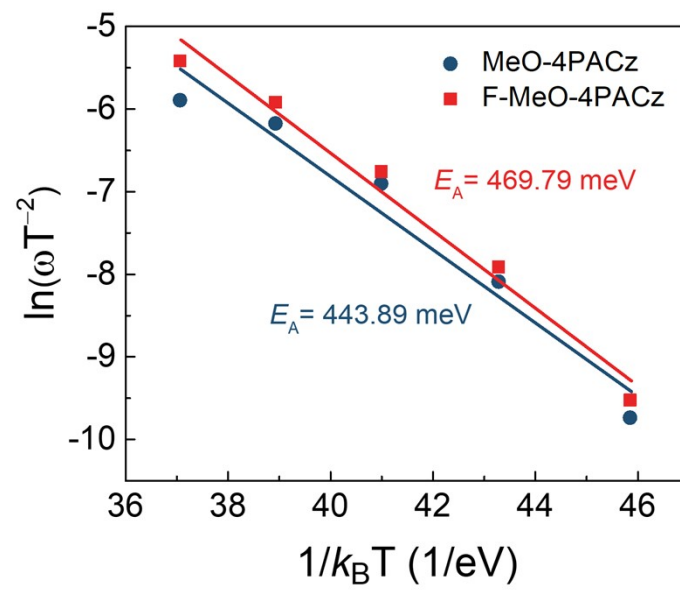


**Fig. S8** Defect activation energy obtained from TAS analysis.

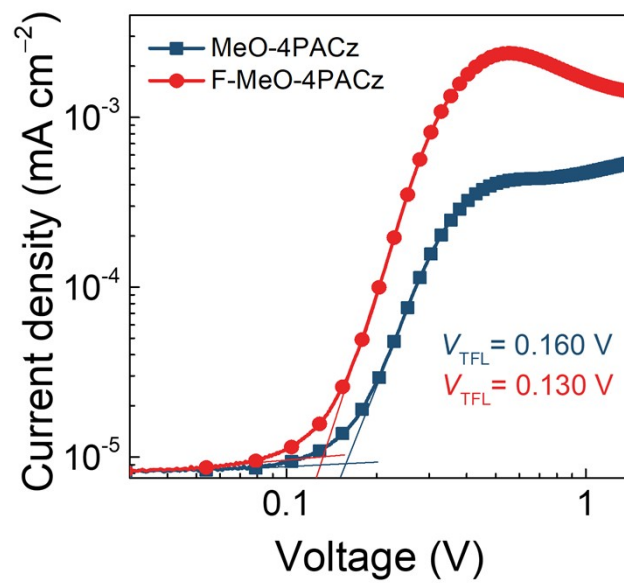


**Fig. S9** SCLC curves of the hole only device (ITO/SAM/perovskite/spiro-OMeTAD/Au).

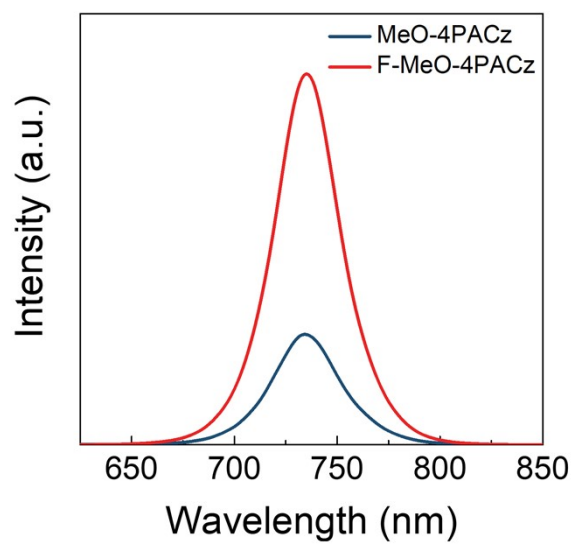


**Fig. S10** SS-PL spectra of the ITO/SAM/perovskite films with different SAMs excited by 520 nm laser from the front side.

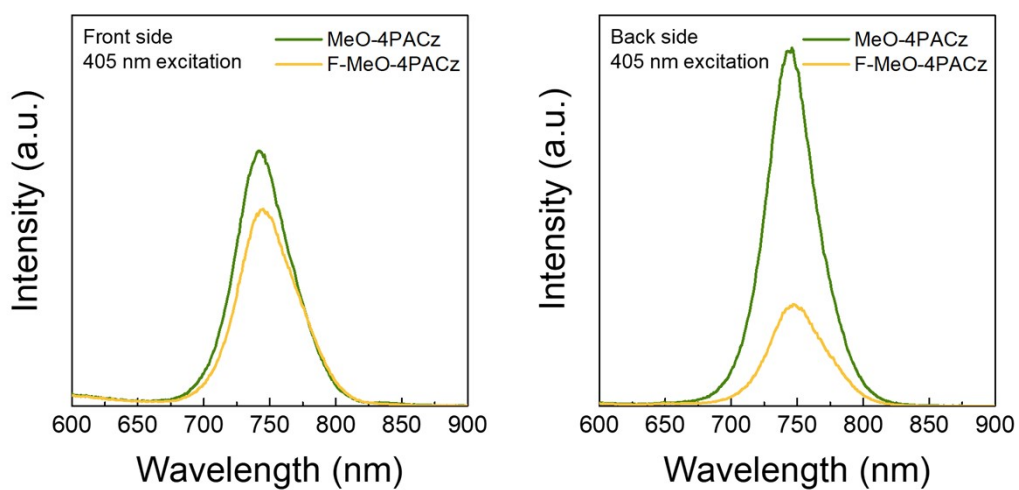


**Fig. S11** SS-PL spectra of the ITO/SAM/perovskite/ $C_{60}$  films with different SAMs according to excitation direction with a 405 nm laser.

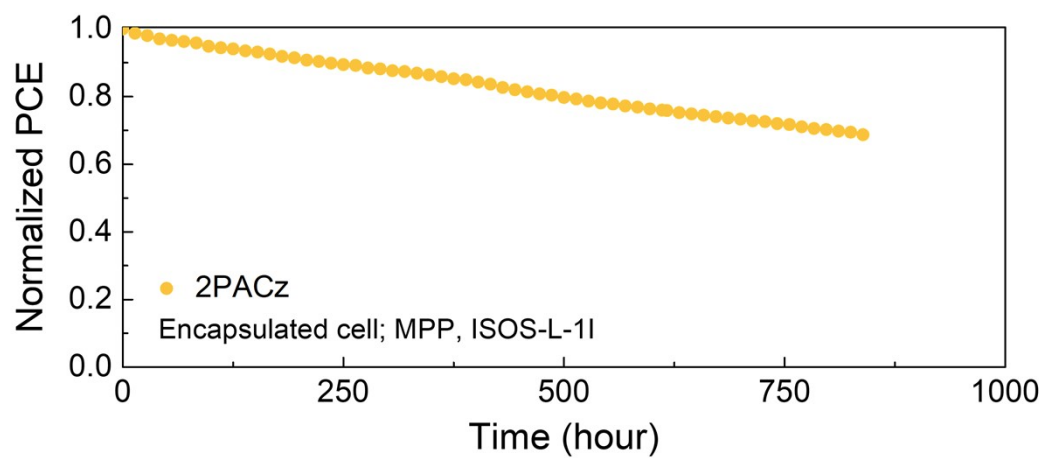


**Fig. S12** Long-term stability of the perovskite single-junction devices incorporating commercial 2PACz under 1-sun illumination with encapsulation (ISOS-L-1I).

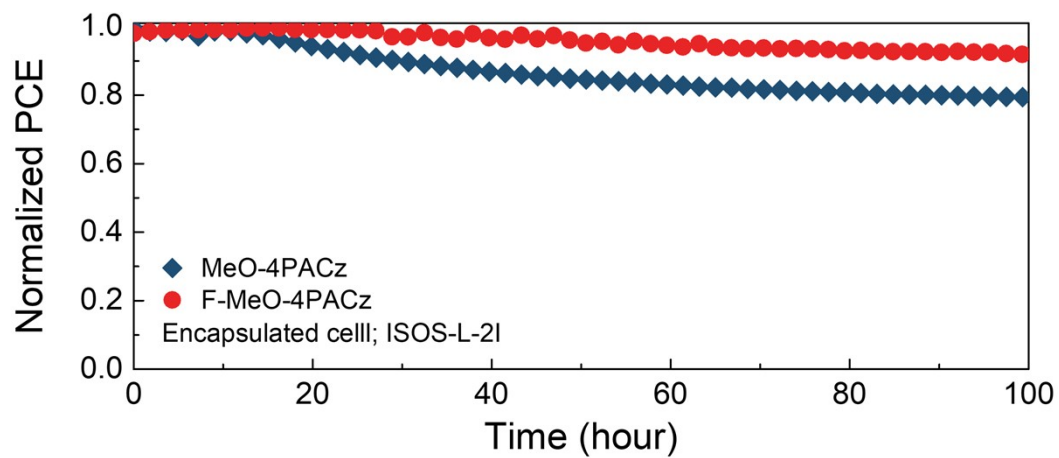


**Fig. S13** Thermal stability of encapsulated single-junction transparent perovskite cells at 65 °C in N<sub>2</sub> atmosphere for 100 h (ISOS-L-2I).

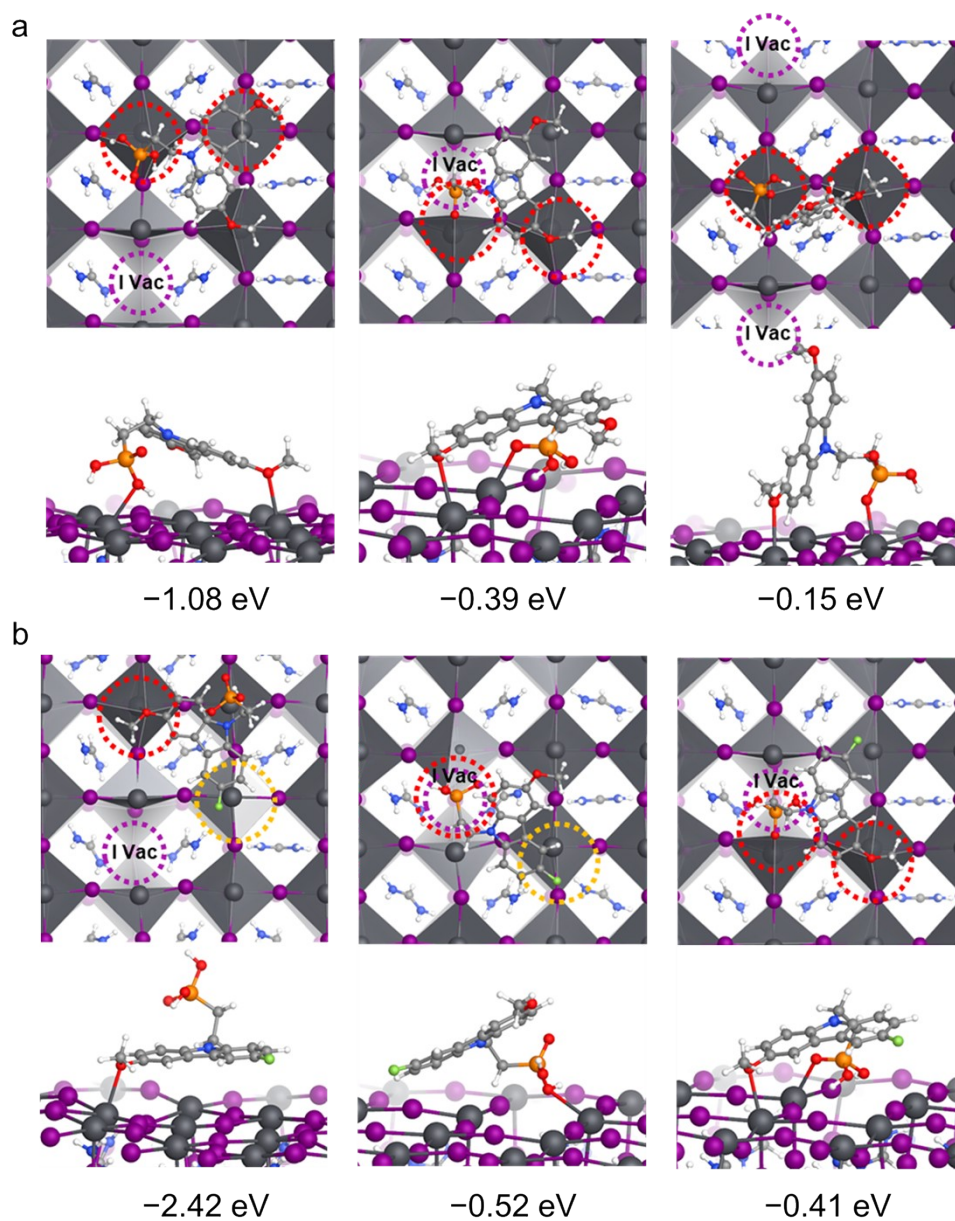


**Fig. S14** Energetically preferred adsorption model of the SAM-perovskite with  $I^-$  vacancies; (a) MeO-4PACz and (b) F-MeO-4PACz.

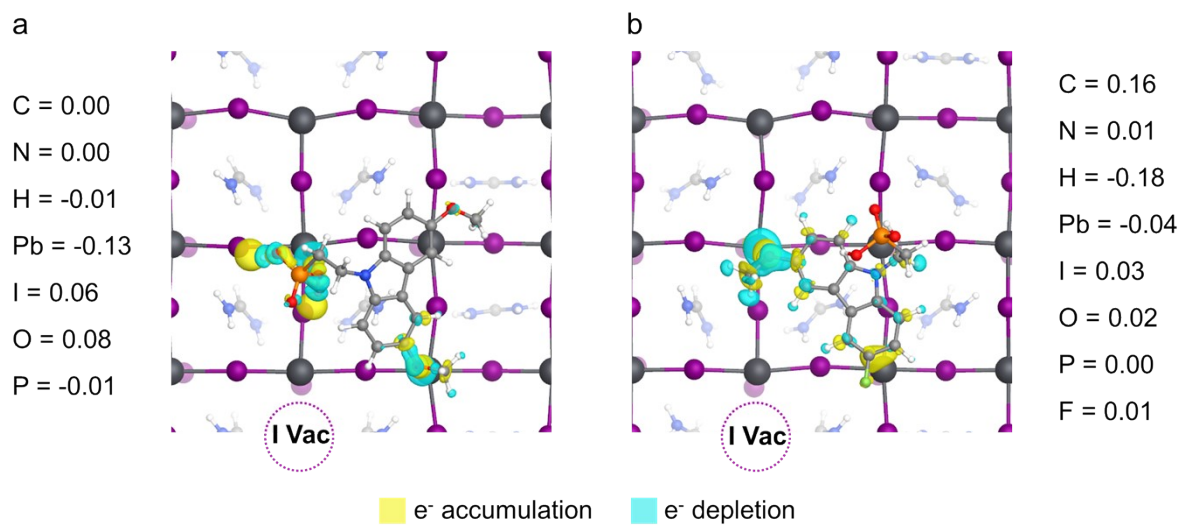


**Fig. S15** Bader charge analysis of the (a) MeO-4PACz and (b) F-MeO-4PACz adsorption with perovskite under I<sup>-</sup> defect condition.

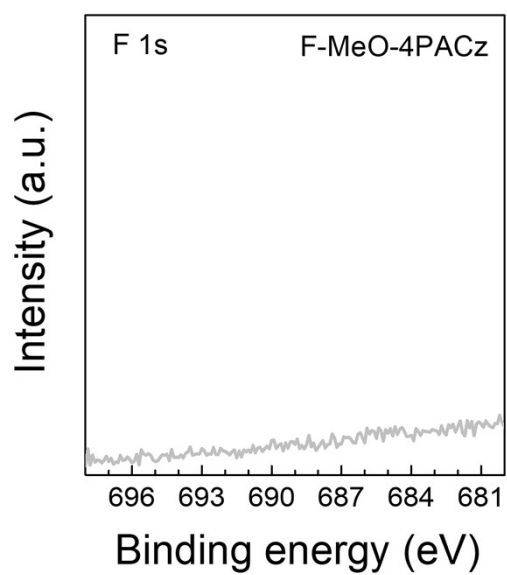


**Fig. S16** XPS spectrum of the F 1s at the perovskite bottom surface that were peeled off from the F-MeO-4PACz/perovskite interface.

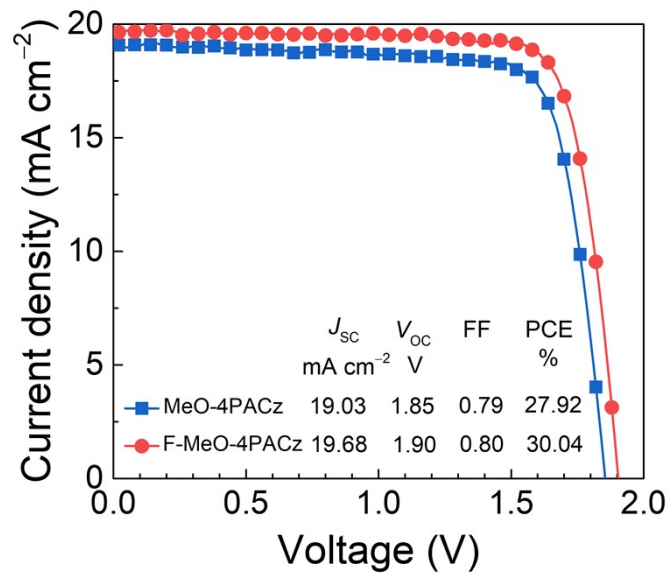


**Fig. S17**  $J$ - $V$  curves of the 2T perovskite/SHJ tandem solar cells with MeO- and F-MeO-4PACz.

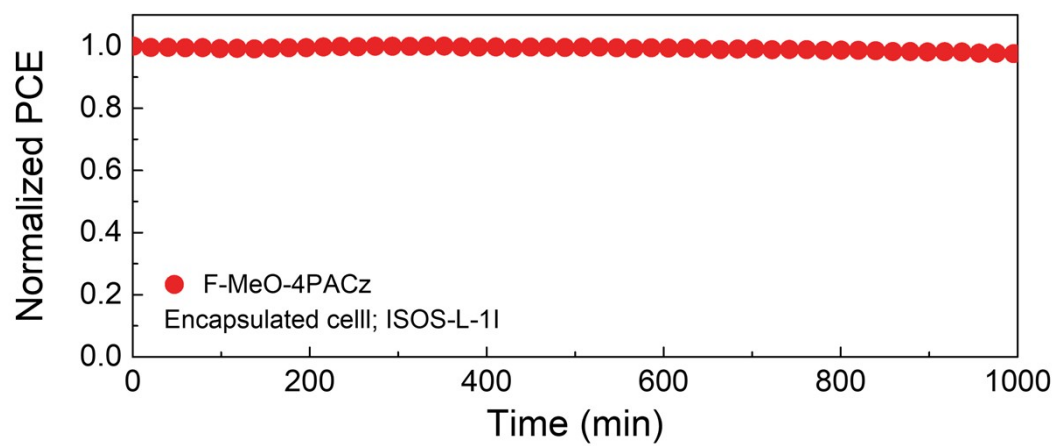


**Fig. S18** MPPT of the encapsulated 2T perovskite/Si tandem cell with F-MeO-4PACz (ISOS-L-11).

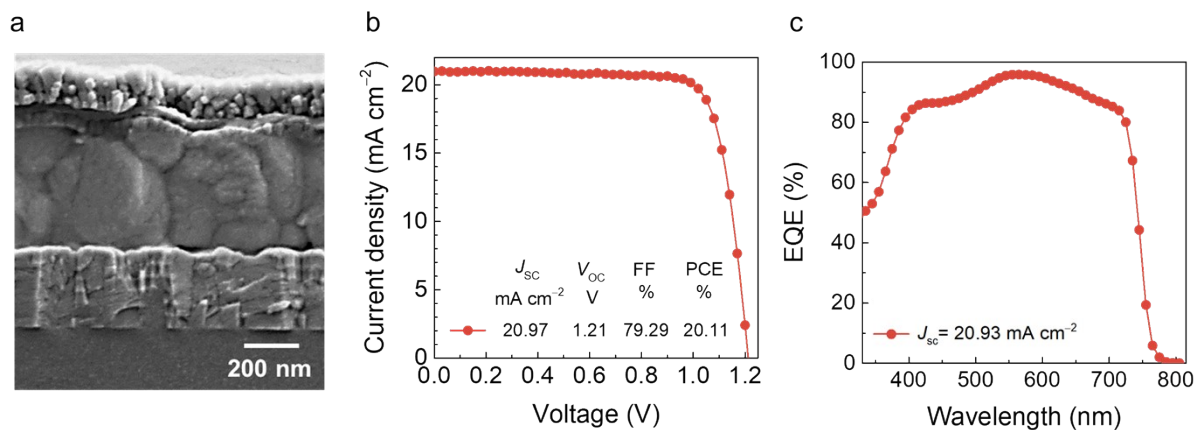


**Fig. S19** (a) Cross-sectional FE-SEM image, (b)  $J$ - $V$  curve, and (c) EQE spectrum of the best-performing semi-transparent perovskite solar cell.

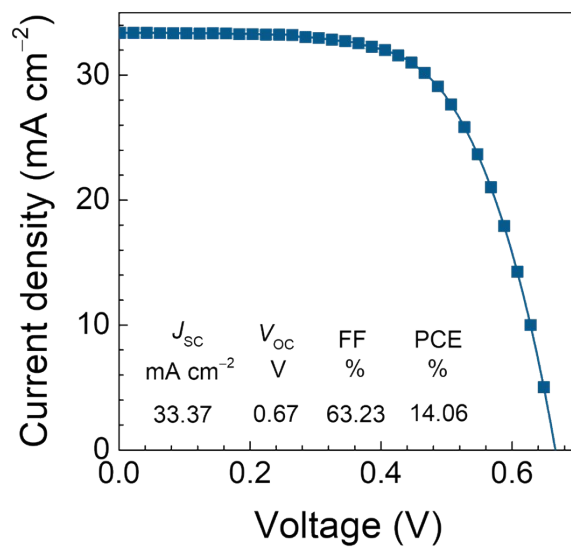


**Fig. S20**  $J$ - $V$  curves of the PERC Si solar cell after removing the perovskite top cell.

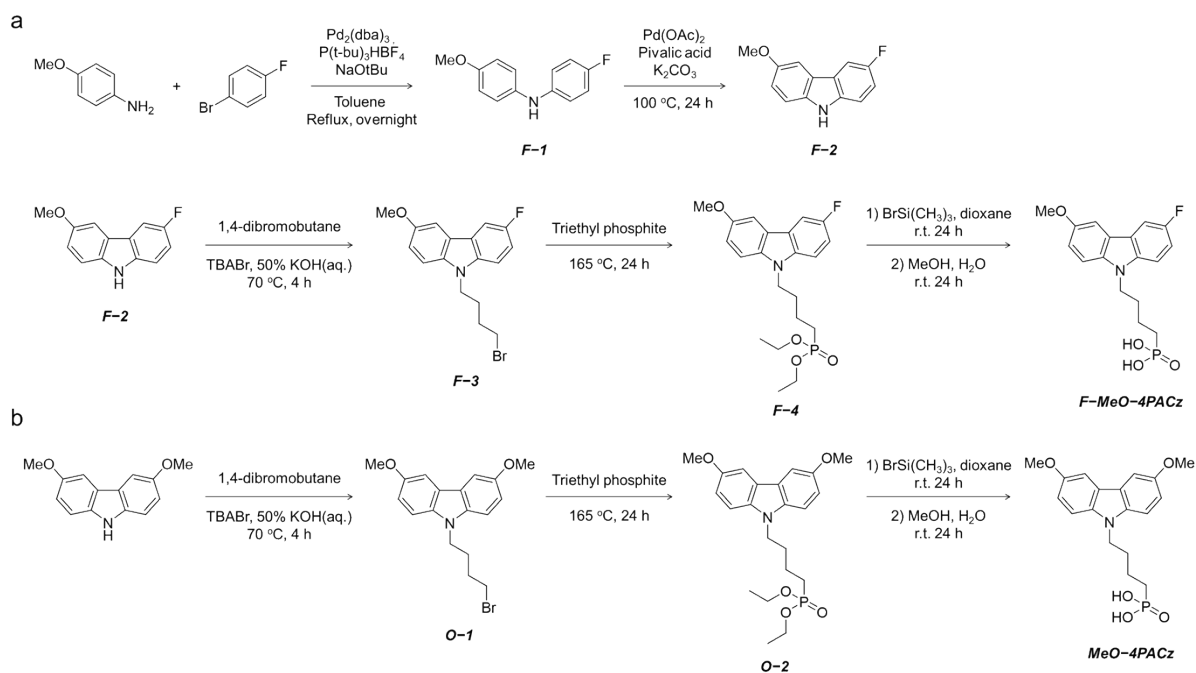


**Fig. S21** Synthesis process of the SAMs molecules for (a) F-MeO-4PACz and (b) MeO-4PACz.

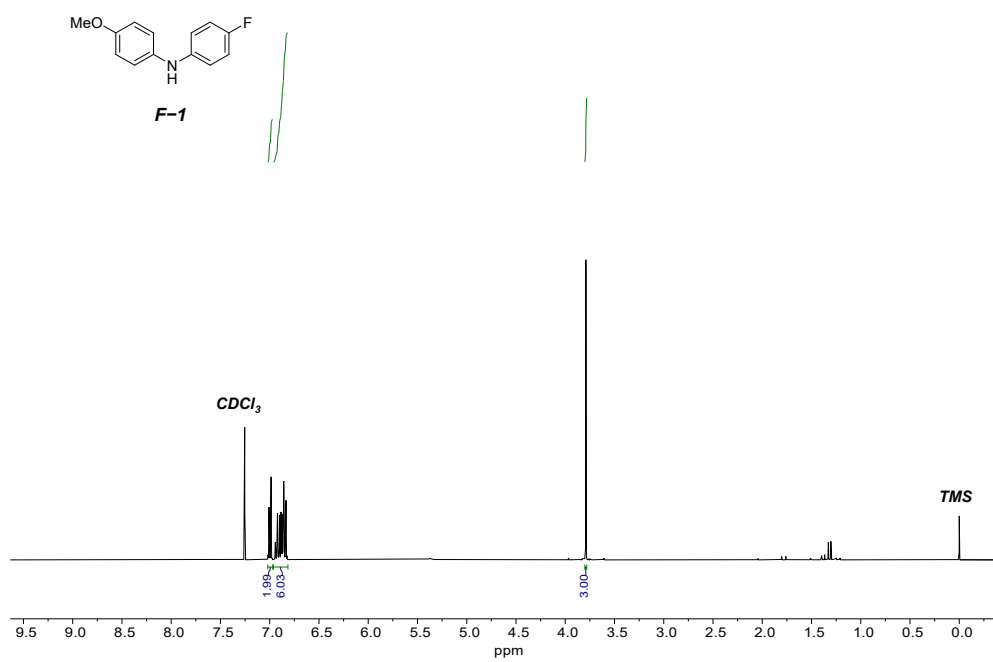


**Fig. S22** <sup>1</sup>H NMR spectrum of 4-fluoro-*N*-(4-methoxyphenyl)aniline (*F-1*).

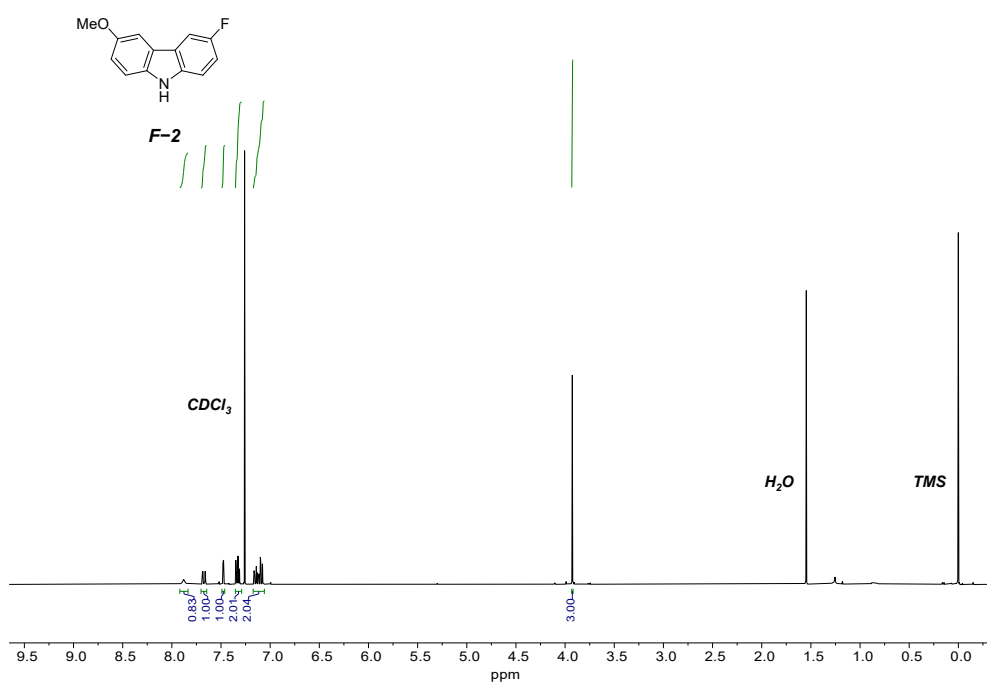


**Fig. S23** <sup>1</sup>H NMR spectrum of 3-fluoro-6-methoxy-9H-carbazole (*F-2*).

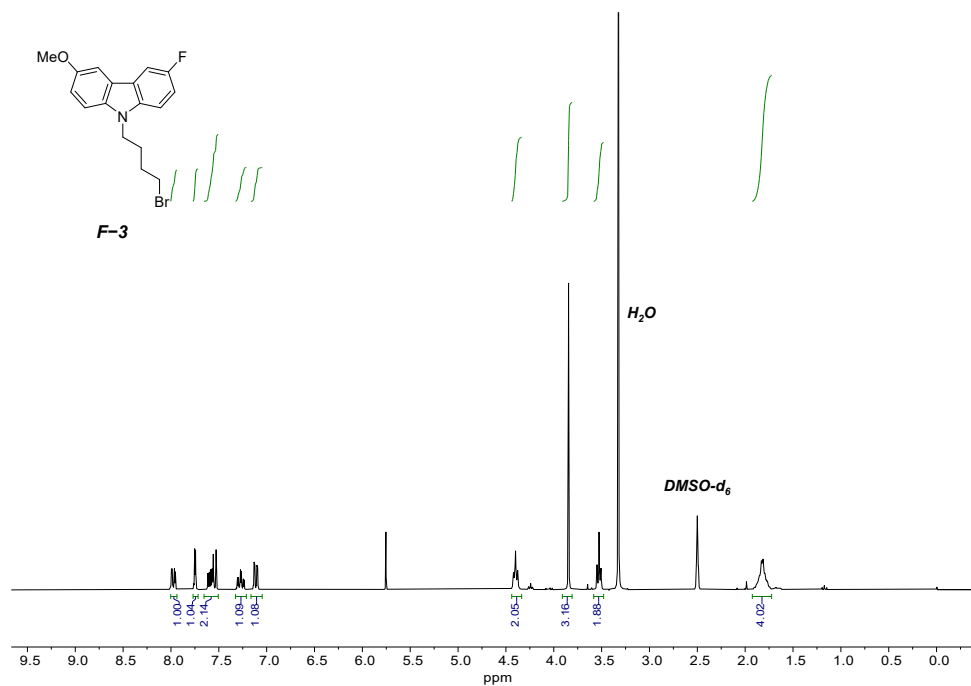


**Fig. S24** <sup>1</sup>H NMR spectrum of 9-(4-bromobutyl)-3-fluoro-6-methoxy-9H-carbazole (**F-3**).

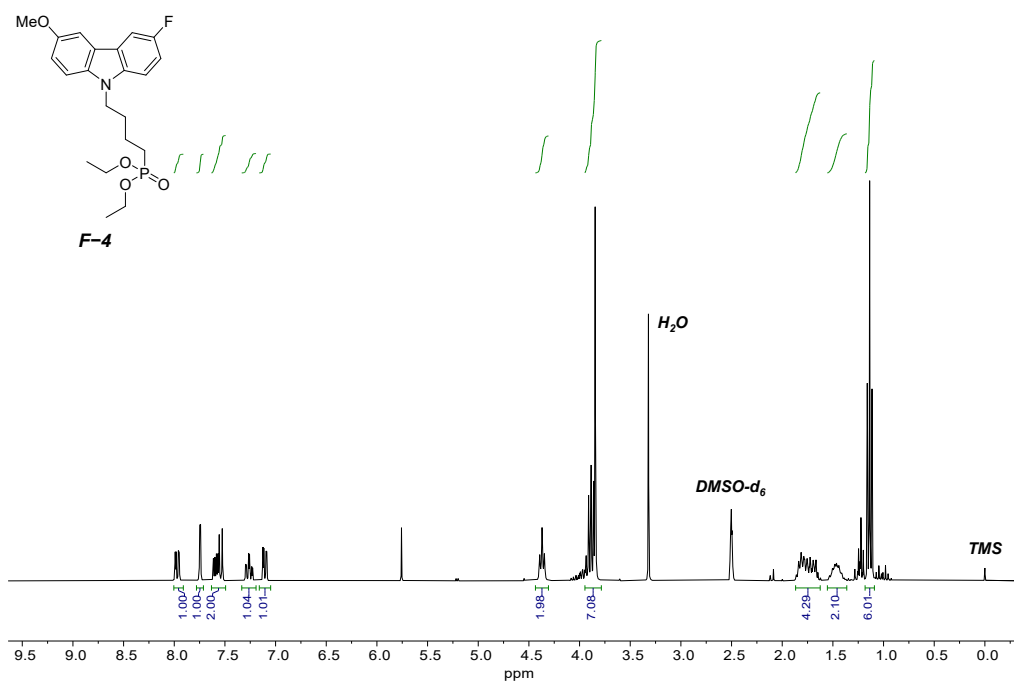


**Fig. S25** <sup>1</sup>H NMR spectrum of diethyl (4-(3-fluoro-6-methoxy-9H-carbazol-9-yl)butyl)phosphonate (**F-4**).

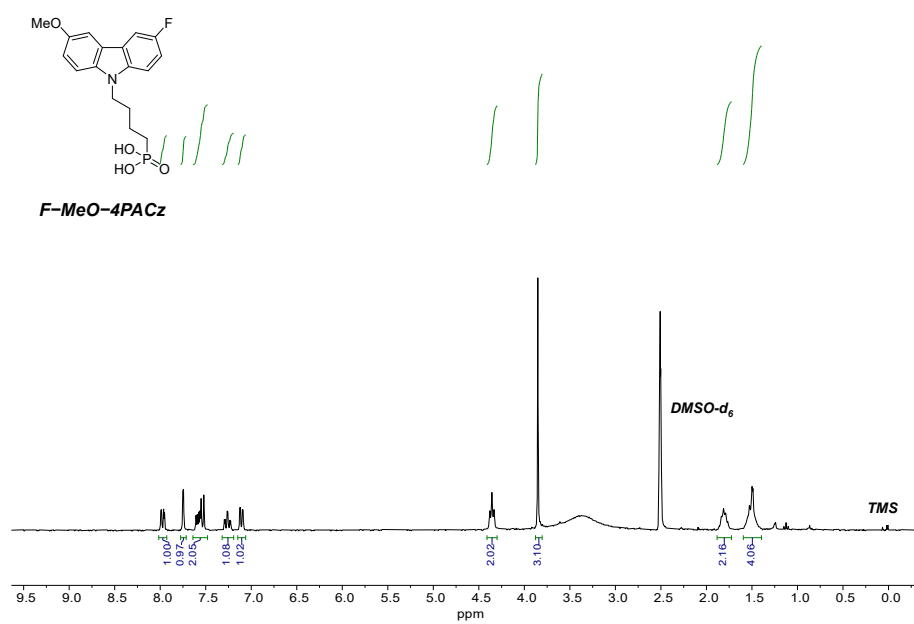


**Fig. S26** <sup>1</sup>H NMR spectrum of (4-(3-fluoro-6-methoxy-9H-carbazol-9-yl)butyl)phosphonic acid (*F-MeO-4PACz*).

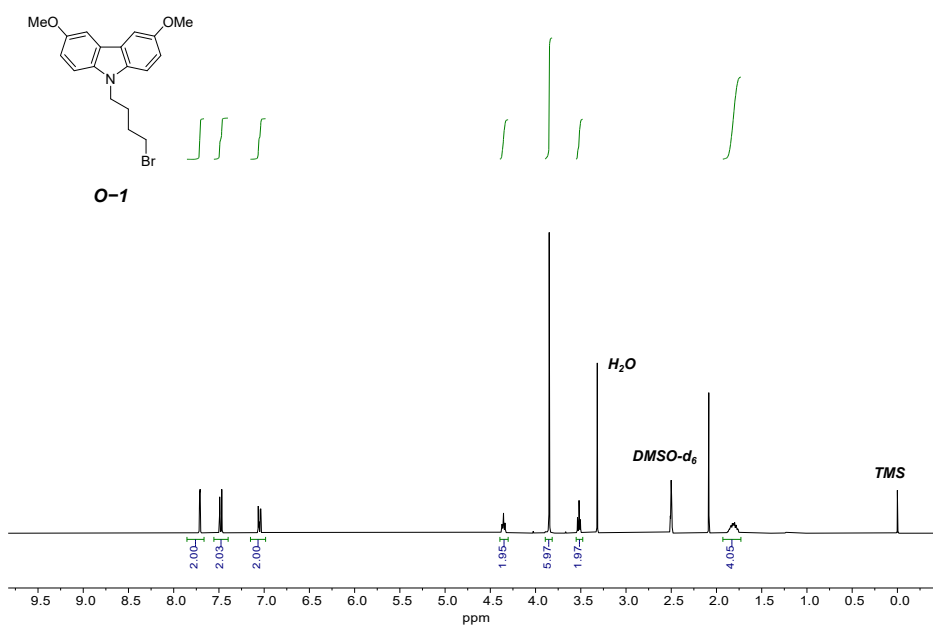


**Fig. S27** <sup>1</sup>H NMR spectrum of 9-(4-bromobutyl)-3,6-dimethoxy-9H-carbazole (**O-1**).

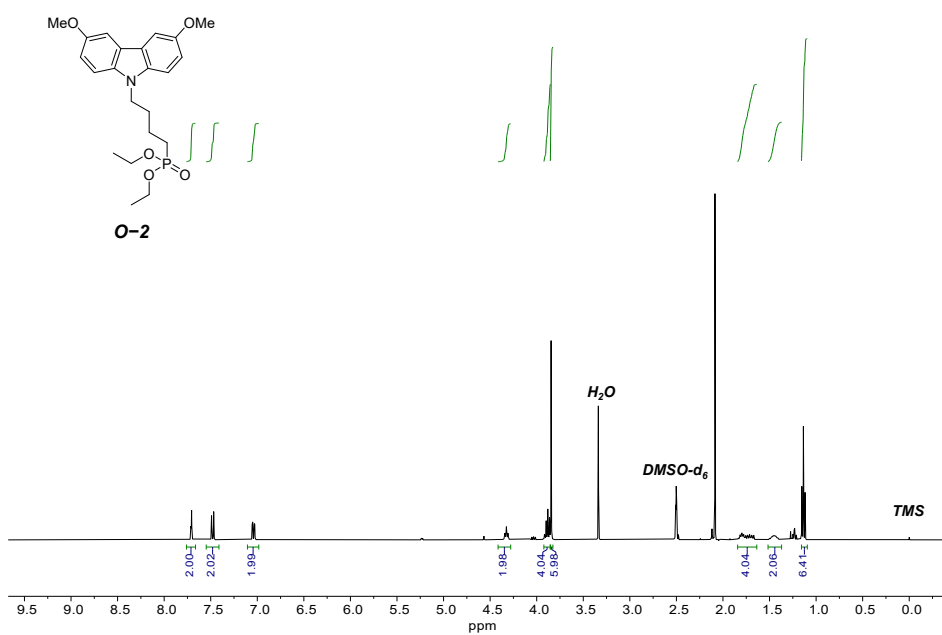


**Fig. S28**  $^1\text{H}$  NMR spectrum of diethyl (4-(3,6-dimethoxy-9H-carbazol-9-yl)butyl)phosphonate (**O-2**).

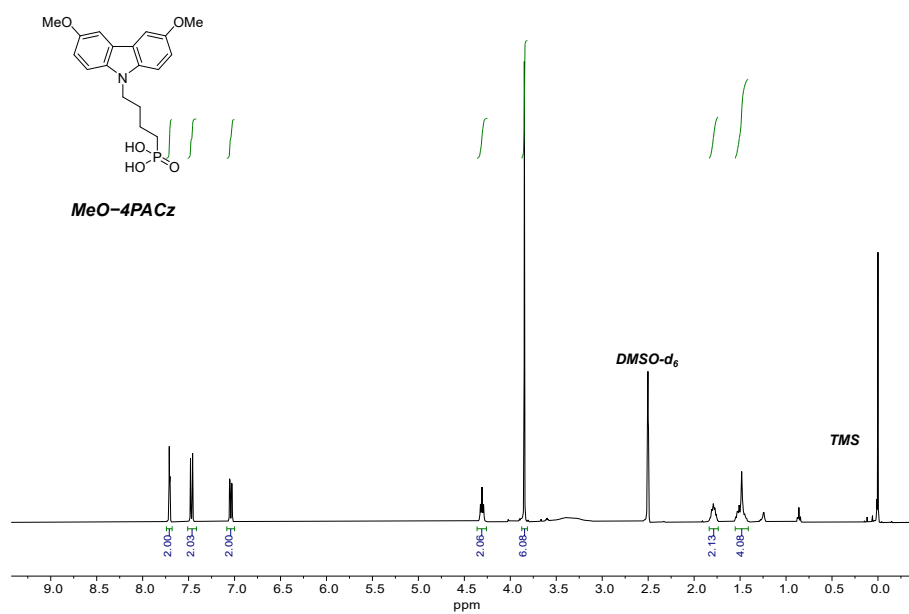


**Fig. S29**  $^1\text{H}$  NMR spectrum of (4-(3,6-dimethoxy-9H-carbazol-9-yl)butyl)phosphonic acid (**MeO-4PACz**).

## Supplementary Tables

**Table S1** Photovoltaic and diode parameters of the perovskite single-junction solar cells with varying substituents

Device	$J_{sc}$ (mA cm <sup>-2</sup> )	$V_{oc}$ (V)	FF	PCE (%)	$G_{sh}$ (S·m <sup>-2</sup> )	$R_s$ (ohm·m <sup>2</sup> )	$n$	$J_0$ (mA cm <sup>-2</sup> )
MeO-4PACz	21.44	1.14	0.81	19.90	1E-7	2.67	1.85	6.32E-7
F-MeO-4PACz	21.23	1.22	0.83	21.62	5E-8	2.24	1.58	5.13E-9

## References

- 1 B. Liégault, D. Lee, M. P. Huestis, D. R. Stuart and K. Fagnou, *The Journal of Organic Chemistry*, 2008, **73**, 5022-5028.
- 2 M. Jeong, I. W. Choi, E. M. Go, Y. Cho, M. Kim, B. Lee, S. Jeong, Y. Jo, H. W. Choi, J. Lee, J.-H. Bae, S. K. Kwak, D. S. Kim and C. Yang, *Science*, 2020, **369**, 1615-1620.
- 3 A. Al-Ashouri, E. Köhnen, B. Li, A. Magomedov, H. Hempel, P. Caprioglio, J. A. Márquez, A. B. Morales Vilches, E. Kasparavicius, J. A. Smith, N. Phung, D. Menzel, M. Grischek, L. Kegelmann, D. Skroblin, C. Gollwitzer, T. Malinauskas, M. Jošt, G. Matic, B. Rech, R. Schlatmann, M. Topič, L. Korte, A. Abate, B. Stannowski, D. Neher, M. Stolterfoht, T. Unold, V. Getautis and S. Albrecht, *Science*, 2020, **370**, 1300-1309.
- 4 G. Kresse and J. Furthmüller, *Physical Review B*, 1996, **54**, 11169-11186.
- 5 T. F. Kellici, D. Ntountaniotis, G. Liapakis, A. G. Tzakos and T. Mavromoustakos, *Arabian Journal of Chemistry*, 2019, **12**, 5062-5078.
- 6 J. C. Slater and J. C. Phillips, *Physics Today*, 1974, **27**, 49-50.
- 7 S. Grimme, *Journal of Computational Chemistry*, 2006, **27**, 1787-1799.
- 8 in *Density Functional Theory*, 2009, DOI: <https://doi.org/10.1002/9780470447710.index>, pp. 235-238.
- 9 I. Fortran, W. Press, S. Teukolsky, W. Vetterling and B. Flannery, *Cambridge, UK, Cambridge University Press*, 1992.
- 10 S. Grimme, J. Antony, S. Ehrlich and H. Krieg, *The Journal of Chemical Physics*, 2010, **132**, 154104.
- 11 K. Momma and F. Izumi, *Journal of Applied Crystallography*, 2011, **44**.